Article ID: 1000-324X(2017)01-0101-06 **DOI:** 10.15541/jim20160210

Synthesis and Physical Properties of Solar Material $Cu_{1-x}Li_xInSe_2$

HUANG Rong-Tie[1, 2], ZHENG Ming[2], SUI Li-Fang[1, 2], CAI Chuan-Bing[1], HUANG Fu-Qiang[2, 3]

(1. Department of Physics, Shanghai University, Shanghai 200444, China; 2. CAS Key Laboratory of Materials for Energy Conversion, Shanghai Institute of Ceramics, Chinese Academy of Sciences, Shanghai 200050, China; 3. Beijing National Laboratory for Molecular Sciences and State Key Laboratory of Rare Earth Materials Chemistry and Applications, College of Chemistry and Molecular Engineering, Peking University, Beijing 100871, China)

Abstract: Bulk materials of Li-doped $Cu_{1-x}Li_xInSe_2$ (x = 0–0.4) were prepared by solid state reaction in evacuated and sealed quartz tubes at 873 K. To understand the physical properties of the materials, the structural, electrical and optical properties were systematically investigated. After doping with lithium, the samples crystallize in chalcopyrite structure with large grain sizes. Electrical resistivity and optical band gap of Li-doped $Cu_{1-x}Li_xInSe_2$ are greatly enhanced to 2.73×10^8 Ω·cm and 1.33 eV from original values of 1.98×10^2 Ω·cm and 0.9 eV, respectively. The large band gap improves the open circuit voltage, indicating that the Li-doping $CuInSe_2$ could be a promising material to future photovoltaic applications.

Key words: chalcopyrite structure; solar cell; bulk material; physical properties; $CuInSe_2$

$CuInSe_2$ (CIS) as a promising candidate for thin film semiconductor solar cells has high absorption coefficient (~10^5 cm^{-1}). Although its optical band gap (1.04 eV) is lower than the optimal gap of ~1.5 eV[1], the corresponding photovoltaic cells can reach the highest efficiency of 20.3%[2]. $CuInSe_2$ and its derivatives have been extensively studied recently[3], however, the previous works were mainly focused on thin films and nanostructures to enhance the photovoltaic behaviors[4-6]. On the other hand, the physical properties of the bulk materials are crucial to explore the intrinsic features, and only few studies concentrated on the physical properties of the bulk materials[7].

Many studies have shown that the electronic band structure can be changed by doping to improve the energy conversion efficiency[8]. The band gap of $CuInSe_2$ increases to 1.2 eV with 30% Ga doping at In site to form $CuIn_{1-x}Ga_xSe_2$ (CIGS) alloy, resulting in the increase of the open circuit voltage of the device. However, the short circuit current decreases largely, and the cell efficiency drops off when $x > 0.3$[9]. It has been observed that Na-doping in the CIS films leads to larger grain sizes, which can reduce boundary scattering and thus increase the carrier mobility[10]. Nevertheless, binary phase would be found on high Na concentrations, and thus decrease the cell efficiency[11]. After doping with lithium, the band gap may be improved to increase the open circuit voltage because of larger band gap of $LiInSe_2$ (2.85 eV)[12] compared to that of $CuInSe_2$ (1.04 eV). Li_2Se is an effective flux for grains growth in many syntheses, which can act not only as a reactant but also a solvent[13]. The increase of electrical resistivity may reduce the loss of current by avoiding the recombination of e-h at the high carrier concentration. Consequently, it is possible to improve the solar cell performance by lithium doping.

Generally speaking, the physical properties of the $CuInSe_2$ and its derivatives are quite sensitive to the preparation conditions, and many methods have been developed to fabricate the bulk materials. The present study mainly focuses on the relationship between the structural and physical properties of the Li-doped $Cu_{1-x}Li_xInSe_2$ (x = 0–0.4) bulk material. In this study, the Li-doped samples were prepared by solid state reaction in a relatively low temperature (873 K) than the reported reaction temperatures (1273–1423 K)[14-15]. And the crystal structure, electrical resistivity and optical characteristics are investigated to understand the improvement of photoelectrical performance.

1 Experimental

1.1 Sample preparation

The following reagents were used as obtained: Cu (Al-

Received date: 2016-03-31; **Modified date:** 2016-05-09
Foundation item: National Natural Science Foundation of China (61376056, 51402341); Science and Technology Commission of Shanghai (13JC1405700, 14520722000); Key Research Program of Chinese Academy of Sciences (KGZD-EW-T06)
Biography: HUANG Rong-Tie (1988–), male, candidate of master degree. E-mail: huangrongtie@student.sic.ac.cn
Corresponding author: HUANG Fu-Qiang, professor. E-mail: huangfq@mail.sic.ac.cn

drich, 99.999%), In (Aldrich, 99.9999%), Se (Alfa Aesar, 99.999%) and Li (Aldrich, 99.9%). Li_2Se, the reactive flux employed in the synthesis, was prepared by the stoichiometric reaction of the elements in liquid NH_3. Cu_2Se and In_2Se_3 were prepared by the reaction of stoichiometric mixtures of elemental copper, indium, and selenium in evacuated and sealed quartz tubes. The series of compounds $Cu_{1-x}Li_xInSe_2$ (x = 0–0.4) were prepared by the reaction of stoichiometric mixtures of Cu_2Se, In_2Se_3 and Li_2Se. The binary reaction mixtures were milled in a mortar, pressed into pellets under an Ar atmosphere in glove box and loaded into evacuated and sealed quartz tubes. The samples were heated to 873 K in 5 h, kept at 873 K for 10 h, and then slowly cooled to room temperature in the furnace. The obtained pellets were cut into approximately 1.0 mm×2.0 mm×6.0 mm rectangular bar samples for fractured surface morphology observation and resistivity measurement, and the pellets were grounded into powders for crystal structure and optical absorbance measurements.

1.2 Characterization

The crystal structure of the samples were characterized by X-ray diffraction measurements (XRD, Bruker D8 ADVANCE, Cu-Kα radiation) and Raman spectra (Thermo Fisher ARL3460) which were measured by using the 532 nm line of an Ar^+ laser beam with a power level of 9 mW. The fractured surface morphologies were studied by scanning electron microscope (SEM, JSM-6510). The electrochemical impedance spectra (EIS) were measured by the electrochemistry working station (CHI660B) with copper foil as electrodes from 0.1 Hz to 100 kHz. The resistivity, ρ, is related to the resistance, R, by: $R=\rho L/S$, where the thickness of the pellet L is 1 mm and the contact area S is 12 mm^2. Optical diffuse reflectance spectra were measured at room temperature by using a UV-Vis-NIR scanning spectrophotometer (Hitachi U-4100, Japan), which used $BaSO_4$ powder as a 100% reflectance standard, over the wavelength range of 500–2500 nm.

2 Results and discussion.

2.1 Structural properties

The XRD patterns of $CuInSe_2$ compound obtained by the reaction of stoichiometric mixtures of Cu_2Se and In_2Se_3, are shown in Fig. 1(a). The sample has the tetragonal chalcopyrite structure (space group I-42d)[16] without any secondary impurity phase such as In_2Se_3 or Cu_2Se. The phase purity is confirmed by the presence of characteristic peaks of (101), (112), (103), (211), (220)/(204), (312)/(116), (008)/(400), (316)/(332) and (325)/(413) in accordance with the standard pattern of JCPDS# 81-1936[17]. Several additional peaks, which could be could be clearly ascribed to the tetragonal chalcopyrite structure as well, are difficult to be identified because of their weak intensities. It is revealed that pure $CuInSe_2$ sample can be prepared at 873 K, which is much lower than the reported 1273 K[14]. At the same time, the pure $CuInSe_2$ sample is identified to have a better crystallinity from the sharp dominant peak of (112) and all the strong peaks.

The Li-doped $Cu_{1-x}Li_xInSe_2$(x = 0–0.4) and the blank sample have nearly the same pattern without impurity phase, indicating that the chalcopyrite structure is preserved after lithium doping with different contents. However, the left shift of the characteristic peaks, especially (316)/ (332) and (325)/ (413) two double peaks, becomes clearer with the increasing Li-doping concentration, as shown in the inset of Fig. 1(a). As shown in Fig. 1(b), this is caused by the increasing lattice parameters of Li-doped samples in accordance with the Bragg equation: $2d\sin\theta = \lambda$. It was observed that more substitution at Cu sites by Li will lead to more lattice disorder[18].

The tetragonal chalcopyrite structure can be characterized by two lattice parameters a and c. The refined lattice parameters calculated from XRD pattern of the blank sample using MDI Jade are a = 0.5785 nm and c = 1.1622 nm, which agree well with those reported previously[19]. The lattice parameters are shifted to larger values with the increasing

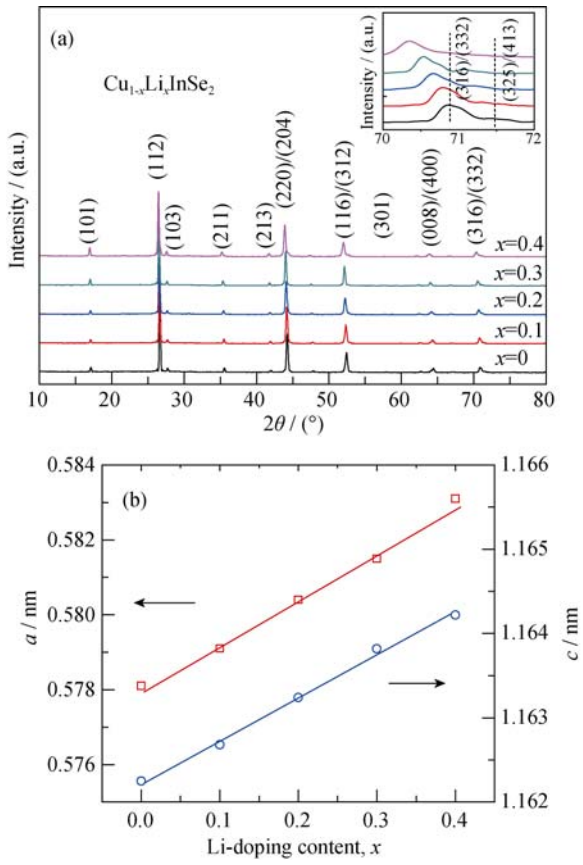

Fig. 1 (a) XRD patterns of $Cu_{1-x}Li_xInSe_2$ (x = 0–0.4) sample (The inset showing details of the XRD patterns around 70° and 72°) and (b) variation of the lattice parameters a and c

lithium content (as shown in Fig. 1(b)). Cu^+ is coordinated by four Se in $CuInSe_2$ of tetragonal chalcopyrite structure, and its radius is 0.060 nm, while the four-coordinated Li^+ is 0.059 nm in the same coordinated site. This has little influence on the obvious shift of (316)/ (332) double peaks if only the difference between radii of Cu^+ and Li^+ is considered, because their radii are close. When Li cations occupies the four-coordinated Cu sites, the highly ionic nature of Li^+ will make the electrostatic interactions between Li and Se much weaker than Cu-Se covalent bonds, resulting in the larger bond length of Li–Se bonds (0.2482 nm) compared with that of Cu–Se bonds (0.2433 nm)[20]. It can conclude that the changes of *a* and *c* lattice parameters are caused by the larger bond length of Li–Se bonds. The increasing trend for the lattice parameters is linear, following Vegard's law, which is in good agreement with previously published data[12].

The typical Raman spectra of $Cu_{1-x}Li_xInSe_2$(x = 0–0.4) samples are presented in Fig. 2. Three Raman modes are detected from 100 to 400 cm^{-1}. The highest peak observed at 172 cm^{-1} for $CuInSe_2$ bulk sample corresponds to the A_1 optical phonon mode in tetragonal chalcopyrite compounds, which is Se–Se vibrational mode[21-22]. The A_1optical phonon mode in $CuInSe_2$ results from the motion of the Se atom, and the Cu and In atoms stay in theoriginal place. The other two weak peaks centered at 210 and 228 cm^{-1} can be assigned to B_2 and B_2, E mode,

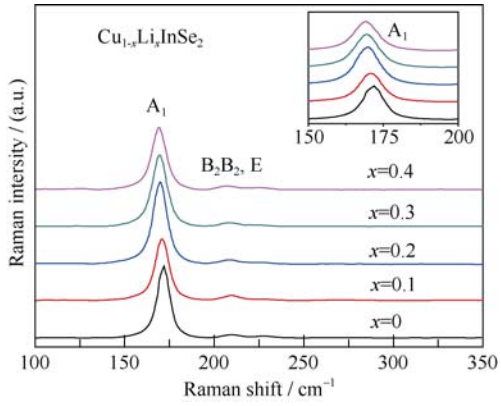

Fig. 2 Typical Raman spectra of $Cu_{1-x}Li_xInSe_2$ (x = 0–0.4) samples
The inset shows details of the Raman spectra from 150 to 200 cm^{-1}

respectively, which are well consistent with the predicted modes in $CuInSe_2$ films[23]. The full width at half-maximum (FWHM) value is about 9 cm^{-1} for $CuInSe_2$ bulk, which is smaller than the typical (FWHM) values of 12–13 cm^{-1} for $CuInSe_2$ thin films[24]. This can be attributed to the higher crystallinity in the bulk $CuInSe_2$ sample.

The A_1 mode shows a redshift with the increasing of Li-doping concentration, as shown in the inset of Fig. 2, which can be attributed to lattice expansion after lithium doping[25]. The FWHM values are similar for the doped samples with different lithium contents, which reveals that the doped samples also have a better crystallinity. These results are consistent with the XRD data. SEM images of fractured surfaces of the as-prepared samples with different lithium contents are shown in Fig. 3. Densely packed grains of all the samples can be observed in spite of some porous structures. The doped samples have well-defined grain structures and larger grain sizes than the blank sample with an average size of about 5 μm. The grain size becomes larger with the increasing lithium content, which is consistent with the molten salt flux mechanism in solid state reaction. In this approach, the flux, Li_2Se, acts not only as a reactant but also as a solvent[13]. Li_2Se has a low melting point below 600℃[26] and will become liquid-phase at high temperature of 873 K. The molten state of Li_2Se helps all the reactants contacting well enough and transporting mass much easier and quicker in crystal growth process than that diffusion in solid state, thus the grains grow much larger. This is in accordance with $CuSbSe_2$-assisted sintering of $CuSb_xIn_{1-x}Se_2$[17]. Therefore, Li_2Se should be good for grains growth. Grains with large sizes can reduce boundary scattering and thus increase the carrier mobility[10], which may improve the performance of solar cell.

2.2 Electrical properties

The typical Nyquist plots of the electrochemical impedance spectra are presented in Fig. 4. All recorded spec tra only include one part in spite of the frequency range, and can be fitted with a semicircle. The intersection with the horizontal axis at higher frequencies is attributed to the grain resistance, while that at lower frequencies corresponds to the sum of the grain resistance and grain boundary

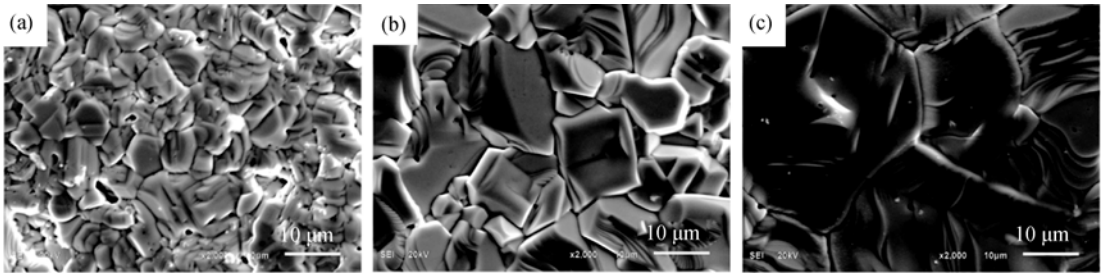

Fig. 3 SEM images of fractured surfaces of $Cu_{1-x}Li_xInSe_2$ (x = 0–0.4) samples
(a) x = 0; (b) x = 0.2; (c) x = 0.4. Bar=10 μm

resistance[27]. As shown in Fig. 4, the radii of these semicircles become much bigger with increasing of Li content, which indicates that the total resistances increase rapidly. Meanwhile, the grain boundary resistances change little at higher frequencies. This means that the grain resistance contributes most to rapidly increasing of total resistance. The electrical resistivity with different doping contents at room temperature is shown in the inset of Fig. 4. The electrical resistivity of the $CuInSe_2$ sample can be greatly increased by lithium doping, from 1.98×10^2 Ω·cm ($CuInSe_2$) to 2.73×10^8 Ω·cm ($Cu_{0.6}Li_{0.4}InSe_2$), showing an exponential dependence of the resistivity on the Li-doping concentration. It may result from that the p-type conduction in $CuInSe_2$ is generally ascribed to intrinsic defects, Cu vacancies (V_{Cu}), which act as dominant shallow acceptor level. However, Li-doping can form interstitial defects (Li_i), acting as donor level[28], which can decrease free hole concentration. Obviously, a sharp increase in electrical resistivity is observed when x increases from 0 to 0.1. It indicates that only small amounts of lithium doping will lead to rapid increase of electrical resistivity of $CuInSe_2$, which can reduce the recombination of e-h and the loss of current at the high carrier concentration to improve the photoelectrical performance.

2.3 Optical properties

In the UV-Vis-NIR diffuse reflectance spectrum, the curve of the absorbance (A) and the wavelength of the incident light (λ) was given. The reflectance (R) can be calculated using the following relation:

$$A = -\lg R \tag{1}$$

The reflectance (R) was converted to F(R) by applying the Munk-Kubelka equation[29]:

$$F(R) = \frac{(1-R)^2}{2R} = \frac{\alpha}{s} \tag{2}$$

F(R) is the Munk-Kubelka function, α is the absorption coefficient, and s is the scattering coefficient. The absorption, which is corresponding to the electron excitation from valance band to conduction band, can be used to determine the optical band gap. $CuInSe_2$ is a direct band-gap semiconductor, and the absorption coefficient (α) is related to the energy band gap (E_g) and the photon energies (hν) as the following equation[30]:

$$(\alpha h\nu)^2 = C(h\nu - E_g) \tag{3}$$

Where C is a constant and h is the *Planck* constant. Therefore, from the plot of squared absorption coefficient $(\alpha h\nu)^2$ *vs* incident photon energy (hν), the value of gap energy (E_g) can be estimated by extrapolating the linear portion of the $(\alpha h\nu)^2$ against hν to the energy axis.

In Fig. 5(a), the absorption behavior of $Cu_{1-x}Li_xInSe_2$ (x = 0–0.4) samples with different contents are presented. The near infrared absorption coefficient of the sample is found to become weaker with the increasing lithium content because of the larger band gap of $LiInSe_2$ (2.85 eV)[12] than that of $CuInSe_2$ (1.04 eV).

The plots of squared absorption coefficient $(\alpha h\nu)^2$ *vs* incident photon energy (hν) for the powder samples doped with different Li concentrations are shown in Fig. 5(b). The measured spectra are similar. These samples are observed to have rather sharp absorption edges, in the same

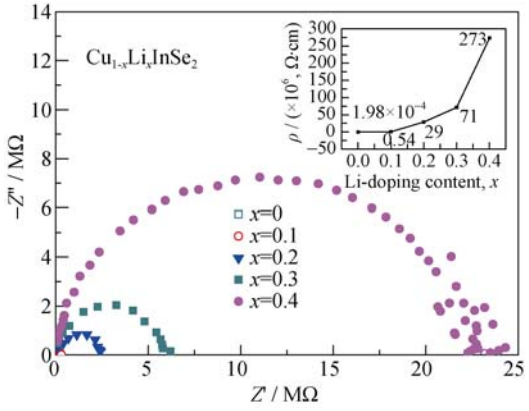

Fig. 4 Typical Nyquist plots of the electrochemical impedance spectra of $Cu_{1-x}Li_xInSe_2$ (x = 0–0.4) samples
The inset shows the electrical resistivity with different doping contents at room temperature

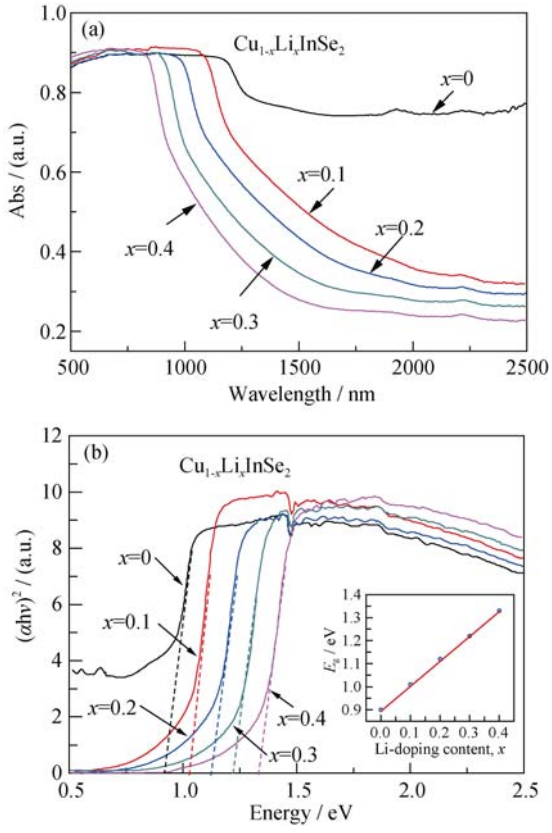

Fig. 5 Diffuse reflectance spectra of $Cu_{1-x}Li_xInSe_2$ (x=0–0.4) samples (a) and the plots of $(\alpha h\nu)^2$ *vs* photon energy for $Cu_{1-x}Li_xInSe_2$ (x=0-0.4) samples (b)
The inset shows the band gaps with different doping contents

energy range as in Fig. 5(a). The linear portions in these plots are quite easy to be identified unambiguously, which adds certainty to the value of band gap. The linear behavior keeps above 0.90 eV for $CuInSe_2$ sample, as shown in Fig. 5(b). Hence, according to the Eq. (3), the value of its band gap is 0.90 eV, which is smaller than that of the reported value (1.04 eV), possibly as a result of its polycrystallinity. The values of band gaps of Li-doping samples can also be determined in the same way. The inset of Fig. 5(b) displays that the optical band gap of $Cu_{1-x}Li_xInSe_2$(x = 0–0.4) varies from 0.90 to 1.33 eV, which increase linearly with the value x. The increasing trend is different from that of $CuIn_{1-x}Ga_xSe_2$(x = 0–1), which is a kind of parabola[31]. The change in these values, as well as some other features of the doped samples, can be understood in terms of the band structure. This may be attributed to the stronger In sp-Se 4p hybridization interaction with the increasing Li-doping concentration, which can reduce the energy of valence band maximum and increase the energy of the conduction band minimum, thus enlarging the energy gap of the doped samples. The band gaps of Li-doped samples are quite close to the optimum value for solar cell applications.

3 Conclusions

In conclusion, $Cu_{1-x}Li_xInSe_2$ (x = 0–0.4) samples have been successfully prepared by the direct reaction of as-prepared binary reaction mixtures in evacuated and sealed quartz tubes at a low temperature. The crystal structure, electrical resistivity and optical absorbance of these Li-doped $Cu_{1-x}Li_xInSe_2$ (x = 0–0.4) samples are systematically studied in comparison with the undoped $CuInSe_2$. All the Li-doped samples crystallize in the chalcopyrite structure with better crystallinity and larger grain size. With the dopant concentration x increases, the electrical resistivity sharply increases from 1.98×10^2 Ω·cm ($CuInSe_2$) to 2.73×10^8 Ω·cm ($Cu_{0.6}Li_{0.4}InSe_2$), and the optical band gaps of 0.90–1.33 eV are obtained. These results indicate that a good photoelectric material can be fabricated Li-doping.

References:

[1] ONUMA Y, TAKEUCHI K, ICHIKAWA S, *et al.* Preparation and characterization of $CuInS_2$ thin films solar cells with large grain. *Sol. Energ. Mat. Sol. C*, 2001, **69(3):** 261–269.

[2] JACKSON P, HARISKOS D, LOTTER E, *et al.* New world record efficiency for Cu(In,Ga)Se_2 thin-film solar cells beyond 20%. *Prog. Photovoltaics*, 2011, **19(7):** 894–897.

[3] CHIANG C S, LEE W H, CHANG T W, *et al.* Improving conversion efficiency of co-electrodeposited $CuInSe_2$ thin film solar cells with substrate and solution heating. *J. Appl. Electrochem.*, 2015, **45(6):** 549–556.

[4] SCHLENKER E, MERTENS V, PARISI J, *et al.* Schottky contact analysis of photovoltaic chalcopyrite thin film absorbers. *Phys. Lett. A*, 2007, **362(2/3):** 229–233.

[5] JAKHMOLA P, AGARWAL G, JHA P K, *et al.* Growth and characterization of chalcopyrite $CuInSe_2$ nanoparticles. *Indian J. Phys.*, 2015, **89(3):** 225–231.

[6] SCHOEN D T, PENG H L, CUI Y. $CuInSe_2$ nanowires from facile chemical transformation of In_2Se_3 and their integration in single-nanowire devices. *ACS Nano*, 2013, **7(4):** 3205–3211.

[7] BEREZNEV S, KOIS J, GOLOVTSOV I, *et al.* Electrodeposited (Cu-In-Se)/polypyrrole PV structures. *Thin Solid Films*, 2006, **511:** 425–429.

[8] HANIAS M, ANAGNOSTOPOULOS A, KAMBAS K, *et al.* On the non-linear properties of Tlins2, Tlinse2, Tlinte2 ternary compounds. *Physica B*, 1989, **160(2):** 154–160.

[9] WEI S H, ZHANG S B, ZUNGER A. Effects of Ga addition to $CuInSe_2$ on its electronic, structural, and defect properties. *Appl. Phys. Lett.*, 1998, **72(24):** 3199–3201.

[10] HAN Q F, LIU Q, DUAN C H, *et al.* Effects of annealing on structural and electrical properties of $CuInSe_2$ thin films prepared by hybrid sputtering/evaporation processes. *J. Electron. Mater.*, 2011, **40(6):** 1452–1456.

[11] WEI S H, ZHANG S B, ZUNGER A. Effects of Na on the electrical and structural properties of $CuInSe_2$. *J. Appl. Phys.*, 1999, **85(10):** 7214-7218.

[12] WEISE S, NOWAK E, LENZ A, *et al*. Investigations of the system $LiInSe_2$-$CuInSe_2$. *J. Cryst. Growth*, 1996, **166(1-4):** 718–721.

[13] SUNSHINE S A, KANG D, IBERS J A. A new low-temperature route to metal polychalcogenides - solid-state synthesis of $K_4T_{i3}S_{14}$, a novel one-dimensional compound. *J. Am. Chem. Soc.*, 1987, **109(20):** 6202–6204.

[14] DJELLAL L, OMEIRI S, BOUGUELIA A, *et al.* Photoelectrochemical hydrogen-evolution over p-type chalcopyrite $CuInSe_2$. *J. Alloys. Compd.*, 2009, **476(1/2):** 584–589.

[15] KLIMOVA A M, ARIF M, TOLOCHKO O V, *et al.* Preparation and properties of copper indium diselenide $CuInSe_2$. *Glass Phys. Chem.*, 2006, **32(3):** 325–329.

[16] KORZUN B V, FADZEYEVA A A, MAROZ I. Phase relations in the $CuInSe_2$-$CuBiSe_2$ semiconductor system. *Phys. Status Solidi C*, 2009, **6(5):** 1047–1050.

[17] YANG C Y, WANG Y M, LI S T, *et al.* $CuSbSe_2$-assisted sintering of $CuInSe_2$ at low temperature. *J. Mater. Sci.*, 2012, **47(20):** 7085–7089.

[18] LIU M L, CHEN I W, HUANG F Q, *et al.* Improved thermoelectric properties of Cu-doped quaternary chalcogenides of $Cu_2CdSnSe_4$. *Adv. Mater.*, 2009, **21(37):** 3808–3812.

[19] PARKES J, TOMLINSO.RD, HAMPSHIR M J. Crystal data for $CuInSe_2$. *J. Appl. Crystallogr.*, 1973, **6(Oct1):** 414–416.

[20] LI Y L, FAN W L, SUN H G, *et al.* Computational insight into the effect of monovalent cations on the electronic, optical, and lattice dynamic properties of $XInSe_2$ (X = Cu, Ag, Li). *J. Appl. Phys.*, 2011, **109(11):** 113535.

[21] MATSUSHITA H, ENDO S, IRIE T. Effects of oxygen doping on bulk properties of $CuInSe_2$ crystals. *Jpn. J. Appl. Phys.*, 1992, **31(9A):** 2687–2688.

[22] ROY S, GUHA P, KUNDU S N, *et al.* Characterization of $Cu(In,Ga)Se_2$ films by Raman scattering. *Mater. Chem. Phys.*, 2002, **73(1):** 24–30.

[23] RINCON C, RAMIREZ F J. Lattice-vibrations of $CuInSe_2$ and $CuGaSe_2$ by Raman microspectrometry. *J. Appl. Phys.*, 1992, **72(9):** 4321–4324.

[24] DAS K, PANDA S K, CHAUDHURI S. Fabrication of nanostructured $CuInS_2$ thin films by ion layer gas reaction method. *Appl. Surf. Sci.*, 2007, **253(11):** 5166–5172.

[25] SPANIER J E, ROBINSON R D, ZHENG F, *et al.* Size-dependent properties of CeO_2-y nanoparticles as studied by Raman scattering. *Physical Review B*, 2001, **64(24):** 245407.

[26] KANATZIDIS M G. New directions in synthetic solid state chemistry: Chalcophosphate salt fluxes for discovery of new multinary solids. *Curr. Opin. Solid St. Mater. Sci.*, 1997, **2(2):** 139–149.

[27] CHIOU B S, LIN S T, DUH J G, *et al*. Equivalent-circuit model in grain-boundary barrier layer capacitors. *Journal of the American Ceramic Society*, 1989, **72(10):** 1967–1975.

[28] SCHON J H. Extrinsic doping of $CuGaSe_2$ single crystals. *J. Phys. D. Appl. Phys.*, 2000, **33(3):** 286–291.

[29] VARGAS W E, NIKLASSON G A. Applicability conditions of the Kubelka-Munk theory. *Appl. Optics*, 1997, **36(22):** 5580–5586.

[30] ALONSO M I, WAKITA K, PASCUAL J, *et al.* Optical functions and electronic structure of $CuInSe_2$, $CuGaSe_2$, $CuInS_2$, and $CuGaS_2$. *Physical Review B*, 2001, **63(7):** 075203.

[31] WEI S H, ZUNGER A. Band offsets and optical bowings of chalcopyrites and Zn-Based Ii-Vi alloys. *J. Appl. Phys.*, 1995, **78(6):** 3846–3856.

太阳能光伏材料 $Cu_{1-x}Li_xInSe_2$ 的合成和物理特性

黄荣铁[1,2], 郑 明[2], 隋丽芳[1,2], 蔡传兵[1], 黄富强[2,3]

(1. 上海大学 理学院, 物理系, 上海 200444; 2. 中国科学院 上海硅酸盐研究所, 中国科学院能量转换材料重点实验室, 上海 200050; 3. 北京大学 化学与分子工程学院, 北京分子科学国家实验室, 稀土材料化学及应用国家重点实验室, 北京 100871)

摘 要: 将原料封装入真空石英管, 在 873 K 进行固相反应制备了 Li 掺杂的 $Cu_{1-x}Li_xInSe_2$ (x = 0–0.4) 块体材料, 并对该材料的结构、电学和光学特性进行了系统性的研究。Li 掺杂之后, 样品的晶体结构还保持黄铜矿结构, 并能得到更大的晶粒。而电阻率从 1.98×10^2 Ω·cm 增大到 2.73×10^8 Ω·cm。光学能隙也从 0.90 eV 提高到 1.33 eV, 增大了光伏开路电压。实验结果表明, Li 掺杂的 $Cu_{1-x}Li_xInSe_2$ 能有效提高光电材料的性能。

关 键 词: 黄铜矿结构; 太阳能电池; 块体材料; 物理特性; $CuInSe_2$

中图分类号: TQ174 **文献标识码:** A